

CREEP PROPERTIES OF GAS METAL ARC DIRECTED ENERGY DEPOSITION AUSTENITIC STAINLESS STEEL

Eun Jang¹, Olivia DeNonno², Juan Gonzales², Jonah Klemm-Toole², Stephen Tate¹

¹Electrical Power Research Institute, Charlotte, NC 28262, USA ²Colorado School of Mines, Golden, CO 80401, USA

ABSTRACT

Gas metal arc directed energy deposition (GMA-DED) has potential for the power generation industry to reduce both time and cost since larger and more complex part geometries can be constructed compared to the typical subtractive methods. The performance of GMA-DED builds can be influenced by the deposition method, resulting microstructure, and formation of defects or secondary phases in the final component. Previous work in the literature evaluated the mechanical properties of GMA-DED builds for a range of austenitic stainless steels, however there is limited data on the high temperature mechanical behavior. This work evaluated the high temperature creep properties of GMA-DED builds constructed with type 316H, 316L, 316LSi, and 16-8-2 stainless steels at 650 °C, 750 °C and 825 °C. The alloy with longest time to rupture for a given stress varied depending on test temperature. Creep damage accumulation at grain boundaries was observed along with grain boundary precipitates which likely aided in damage accumulation. Evaluating the creep properties with the Larson-Miller parameter showed the majority of results fell within the scatter band of creep performance for wrought 316 alloys, indicating the GMA-DED process may be suitable for use in advanced energy systems.

Keywords: Creep, Manufacturing and Fabrication, Metallography/Microscopic/Microstructure, Pressure Vessels, Weld/Welding

1. INTRODUCTION

Additive manufacturing (AM) is being investigated as a fabrication method for pressure retaining components in power generation applications. AM allows for the rapid production of unique and complex components at shortened lead times and reduced costs. AM processes like gas-metal arc directed energy deposition (GMA-DED) utilize welding wire feedstock and high deposition rates to produce large-scale components with minimal material waste making it the optimal process for the fabrication of new or replacement components for power generation [1].

Austenitic stainless steels are commonly used in power generation due to their combination of good corrosion resistance and strength and ductility at elevated temperatures. Austenitic stainless steels are also considered weldable, making them a good option for GMA-DED which can be equated to a multi-pass welding process.

Type 316L and 316H austenitic stainless steels are commonly used for power generation components, where 316H has increased carbon content leading to increased precipitation of $M_{23}C_6$ carbides for greater elevated temperature strength and creep resistance [2]. 316H is used for high temperature and pressure retaining components which are commonly welded using 16-8-2 weld filler. Type 16-8-2 is an austenitic stainless steel weld filler that is compositionally lean with reduced chromium and molybdenum content to prevent the formation of embrittling secondary phases like σ phase [2–4]. Type 16-8-2 also has increased carbon content similar to 316H to promote the formation of $M_{23}C_6$ carbides. Good high temperature properties paired with limited secondary phase formation indicates 16-8-2 could also make a promising GMA-DED alloy.

Type 316LSi is a higher silicon version weld filler of 316L which is used to enhance the fluidity of melt pool [2]. Hagen *et al.* performed tensile testing on GMA-DED austenitic steels and reported increased ultimate tensile strength and ductility for 316LSi compared to 316L [5]. Gonzalez *et al.* reported ultimate tensile strengths of GMA-DED 316LSi similar to GMA-DED 316H at room temperature and 650 °C [6]. Types 16-8-2 and 316LSi demonstrate promising material properties as weld fillers, but are not produced in wrought form [3,5]. The GMA-DED process opens the alloy space of austenitic stainless steel by allowing components to be produced using conventional alloys like 316L and 316H as well as non-conventional alloys like 16-8-2 and 316LSi.

Power generation components have long service lives at elevated temperatures, necessitating the need to understand the creep behavior of GMA-DED stainless steel. Smith *et al.* analyzed the creep performance of 300 series austenitic stainless steel weldments and determined that a number of different

This work was prepared while under employment by the government of a non-US government agency as part of the official duties and as such Copyright is owned by that government, which reserves its own Copyright under national law.

factors such as carbon and nitrogen content, welding process, precipitation type, and δ -ferrite amount control creep properties. It was shown that weldments with high amounts of δ -ferrite resulted in increased embrittlement leading to drastically reduced creep ductility. A reduction in creep ductility was also observed for increasing silicon content of 316 weldments [3]. Ward compared the creep performance of austenitic stainless steel weld material to wrought material and found an overall trend of reduced rupture times for the weld material compared to wrought. The reduced creep life was correlated to higher minimum creep rates and reduced creep ductility of weld material compared to wrought material [7]. Morris et al. analyzed the creep behavior of 316L to determine the creep deformation mechanisms over a range of stresses and temperatures. Between 575 °C and 900 °C, at stresses leading to creep lives of 100 to over 1,000 hours, creep behavior was associated with dislocation creep mechanism where dislocation motion is thermal assisted by diffusion of vacancies to overcome barriers. A power law relationship between minimum creep rate and stress indicated stress exponents between 6 to 12 are associated with a dislocation creep mechanism for 316L [8].

There is limited work in the literature related to the creep behavior of AM stainless steels, with available investigations limited to the creep performance of 316L produced using the laser powder bed fusion (L-PBF) process. Li *et al.* and Calderón *et al.* investigated the creep behavior of L-PBF 316L compared to wrought 316L while William *et al.* investigated impact of build direction on creep performance [9–11] . For DED processes, there is a lack of literature on the creep performance of stainless steel alloys. Compared to the L-PBF process, DED processes have slower cooling rates resulting in larger grain sizes and increased grain texture which will result in different if not enhanced creep properties compared to the finer grained L-PBF material. Therefore, it is of interest to investigate the creep performance of GMA-DED stainless steel and provide data that is lacking in current literature.

In this present work, four common austenitic stainless steel weld filler metals used in power generation applications, 316L, 316LSi, 316H, and 16-8-2, were used to produce GMA-DED builds. The creep performance of the alloys was investigated at 650 °C, 750 °C, and 825 °C, and the creep damage was characterized. The creep performance of the GMA-DED stainless steel alloys was compared to wrought 316H using a Larson-Miller plot indicating GMA-DED as a promising method for production of creep limited components.

2. MATERIALS AND METHODS

2.1 Material Fabrication

A GMA-DED set-up consisting of a Universal Robot UR10e collaborative robot and a Fronius TPS 400i gas metal arc welding (GMAW) power source was used to fabricate walls using 1.14 mm (0.045") diameter 316L, 316LSi, 316H, and 16-8-2 welding wire. Three bead wide rectangular walls approximately 254 mm long x 102 tall x 25 mm thick were fabricated using the cold metal transfer (CMT) weld mode and a weaving weld strategy

with a 3 mm pitch and 7.5 mm width. All builds were fabricated with a travel speed of 4 mm/s (9.4 in/min), a wire feed rate of 83 mm/s (195 in/min), and a 95% Ar + 5% CO_2 shielding gas mixture with a flow rate of approximately 11.8 liters per minute (25 cubic feet per hour). As-deposited build compositions are presented in Table 1.

The walls were sectioned away from the 304 baseplate and solution annealed at 1040 °C for 1 hour followed by a water quench per ASTM A480/A480M [12]. The solution annealed walls were then machined into 9.5 mm diameter x 47.6 mm gauge length round creep samples orientated horizontal to the build direction.

2.2 Creep Testing

Creep testing was performed for each stainless steel alloy. Short-term creep testing targeted lifetimes less of than 500 hours while longer-term creep testing targeted lifetimes of approximately 1000 hours based on wrought 316H creep behavior. Longer-term creep testing was performed at 650 °C at 160 MPa, 750 °C at 65 MPa, and 825 °C at 35 MPa using an ATS lever arm creep frame. Short-term creep testing was performed at 650 °C at 155 MPa (316L), 650 °C at 185 MPa, 650 °C at 200/210 MPa (16-8-2/316LSi, 316H), and 650 °C at 245 MPa using a Zwick Roell electro-mechanical testing frame.

2.3 Microstructure Characterization

Sections from the builds after solution annealing were characterized using electron backscatter diffraction (EBSD). EBSD was performed using a Helios NanoLab 600i scanning electron microscope (SEM) equipped with an EDAX Hikari Super detector with a 20 kV accelerating voltage. High magnification imaging was performed with a TENEO SEM equipped with a backscattered electron (BSE) detector and analysis of secondary particles was performed using an Oxford Ultim Max EDS detector.

Bulk chemical composition was determined with optical emission spectrometry per ASTM E1086-22 [13] and nitrogen, carbon, and oxygen content was determined with combustion and inert gas fusion per ASTM E1019-18 [14]. The chemical composition results of the builds are presented in [6]. In general, negligible changes in composition were observed between the wire and build compositions.

TABLE 1. AS-BUILT WALL COMPOSITION OF GMA-DED BUILDS (wt%).

(•, •,•			
	316L	316LSi	316H	16-8-2
C	0.03	0.03	0.05	0.05
N	0.049	0.065	0.064	0.040
O	0.034	0.022	0.039	0.031
Cr	18.39	18.19	18.79	15.37
Ni	12.13	11.43	11.30	8.35
Mo	2.12	2.36	2.11	1.11
Mn	1.63	1.70	1.81	1.40
Si	0.35	0.85	0.34	0.41
P	0.024	0.017	0.017	0.013
\mathbf{S}	0.013	0.012	< 0.005	< 0.005
Fe	Bal.	Bal.	Bal.	Bal.

2.4 Phase Stability Predictions

Phase stability as a function of temperature was determined using the single-axis equilibrium module of Thermo-Calc version 2023b using the TCFE12 v12.0 database. Single-axis equilibrium simulations were performed using the build compositions reported in [6]. Oxygen and sulfur were not included in the simulations. Predicted equilibrium phase amounts at 650 °C, 750 °C, and 825 °C were used to interpret phase stability and microstructure evolution during creep.

3. RESULTS AND DISCUSSION

3.1 Starting Microstructure and Predicted Phase Stability

EBSD phase maps of the solution annealed microstructure of each stainless steel alloy are shown in Figure 1. Residual δ -ferrite from the deposition process is observed for all alloys indicating a one-hour solution anneal at 1040 °C is insufficient for full dissolution of δ -ferrite that formed during solidification. The presence of small amounts of δ -ferrite likely has a minimal impact on the creep performance of the stainless steel alloys.

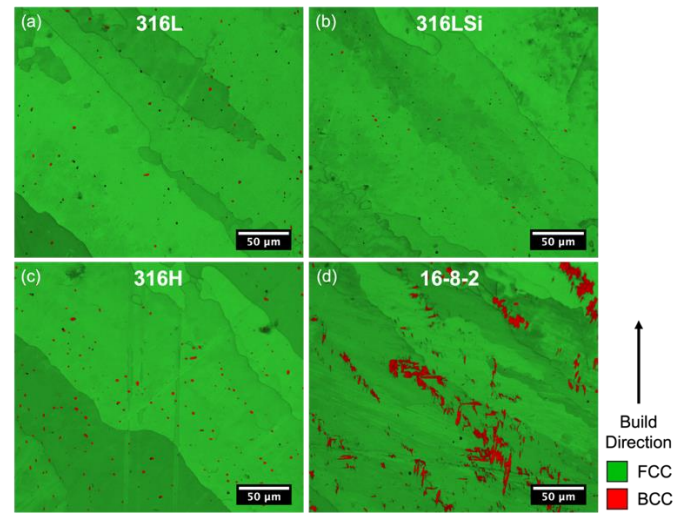


FIGURE 1. EBSD PHASE MAPS OF SOLUTION ANNEALED (a) 316L, (b) 316LSi, (c) 316H, AND (d) 16-8-2.

The results from the single-axis equilibrium Thermo-Calc simulations are shown in Table 2. For 316L, 316LSi, and 316H a considerable amount of σ phase is predicted to be stable at 650°C along with smaller amounts of laves, η , and $M_{23}C_6$ carbides. At the increased testing temperatures of 750 °C and 825 °C, slightly less σ phase is predicted to be stable while similar amounts of η and $M_{23}C_6$ as at 650 °C are expected.

For 16-8-2, which is designed specifically to be lean in alloying elements to prevent the formation of σ phase at elevated temperatures, no σ phase is predicted at any testing temperature. The major difference in phase stability among these alloys is the stability of ferrite in 16-8-2 at $650\,^{\circ}\text{C}$. The unexpected stability of ferrite at $650\,^{\circ}\text{C}$ can be rationalized by the lean alloy composition of 16-8-2. It is possible that during long term creep testing of 16-8-2 at $650\,^{\circ}\text{C}$ ferrite can form and impact creep performance. Similar to 316H, 16-8-2 maintains its strength at elevated temperatures through $M_{23}C_6$ precipitation where around 1 vol. % is predicted for both alloys for all testing temperatures. For 316L and 316LSi, less $M_{23}C_6$ precipitation is predicted, approximately $0.5\,^{\circ}\text{vol}$ % at all testing temperatures, indicating elevated temperature strength may be lower.

TABLE 2. EQUILIBRIUM PHASE AMOUNT (VOLUME %) PREDICTED AT CREEP TESTING TEMPERATURES OF 650 °C, 750 °C, AND 825 °C USING BULK ALLOY COMPOSITION

		Ferrite	Laves	η	M23C6	σ
650°C	316L	0	2.5	1.0	0.5	14.2
	316LSi	0	3.0	1.8	0.6	13.2
	316H	0	2.2	1.7	1.0	13.4
	16-8-2	9.8	1.0	1.0	1.0	0
750°C	316L	0	0.1	0.9	0.5	11.6
	316LSi	0	0.4	1.8	0.6	10.9
	316H	0	0	1.4	1.0	11.5
	16-8-2	0	0	0.6	0.9	0
825°C	316L	0	0	0.5	0.4	6.2
	316LSi	0	0	1.6	0.5	6.5
	316H	0	0	0.8	0.9	5.9

3.1 Creep Performance of GMA-DED Austenitic Stainless Steels

Creep curves showing creep strain as a function of time are shown in Figure 2. At 650 °C (Fig. 2a – 2c), 316LSi and 316H exhibit increased creep life and creep ductility across applied stress conditions while 16-8-2 and 316L exhibit reduced creep life comparatively. At 750 °C and 825 °C (Fig. 2d and 2e), a shift in creep performance is observed where 16-8-2 exhibits the best elevated temperature creep performance while 316LSi exhibits the worst. 316H exhibits good creep ductility and creep life over the range of testing temperatures.

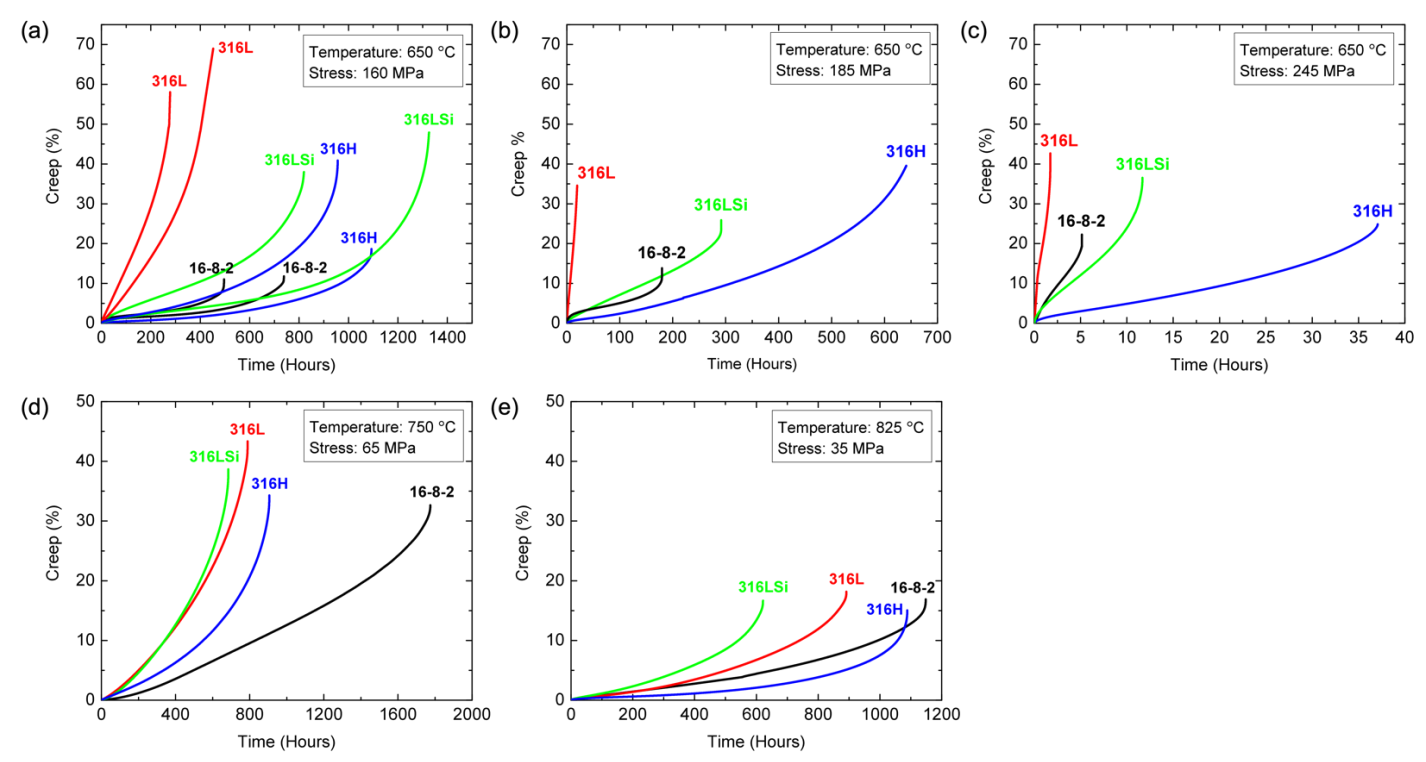


FIGURE 2. CREEP CURVES OF CREEP STRAIN VERSUS TIME FOR 316L, 316LSi, 316H, AND 16-8-2: (a) 650 °C AT 160 MPa, (b) 650 °C AT 185 MPa, (c) 650 °C AT 245 MPa, (d) 750 °C AT 65 MPa, AND (e) 825 °C AT 35 MPa.

The disparity in creep performance of 16-8-2 at 650 °C compared to 750 °C and 825 °C is likely related to the change in ferrite stability of 16-8-2. As shown in Table 2, ferrite is stable at 650 °C indicating it can form during creep and contribute to the reduced creep performance of 16-8-2. When ferrite is no longer stable at 750 °C and 825 °C, 16-8-2 exhibits superior creep performance. Body centered cubic (BCC) ferrite has a higher diffusivity than closed-packed face centered cubic (FCC) austenite leading to enhanced dislocation climb. Sherby and Burke showed that the minimum creep rate of α -iron (BCC) is 200 times greater than that of γ -iron (FCC) due to self-diffusion in α -iron being 350 times greater than in γ -iron at 910 °C [15]. The increased diffusivity of ferrite likely resulted in the reduced creep performance of 16-8-2 at 650 °C. Recently, DeNonno et al. also reported the presence of ferrite and athermal martensite in 16-8-2 after creep testing at 650 °C through high magnification EBSD [16].

The formation of ferrite in 16-8-2 during long-term creep appears to have a greater impact on creep performance at 650 °C than σ phase formation seeing as approximately 13 vol % σ phase is predicted for 316LSi and 316H, but both alloys exhibited superior creep life and creep ductility. The formation of σ phase during elevated temperature aging or long-term creep testing is commonly associated with reduced ductility and embrittlement. Smith *et al.* note that the amount, distribution, and morphology of σ phase dictates the impact it has on high temperature properties [3]. For 316LSi and 316H it appears the

 σ phase formation at 650°C had minimal impact on creep properties.

Both 16-8-2 and 316H retain elevated temperature strength through around 1 vol. % M₂₃C₆ precipitation. For 316H, this resulted in the best overall creep performance over the range of testing temperatures while for 16-8-2, the enhanced creep performance was only observed at elevated temperatures where ferrite was not stable. For 316L and 316LSi, less M₂₃C₆ precipitation is predicted, around 0.5 vol. %, which likely resulted in reduced creep performance of 316L over all testing temperatures. For 316LSi increased creep performance is observed at 650 °C while at 750 °C and 825 °C, 316LSi performs the worst. Increased tensile strength and elongation have been observed for 316LSi compared to 316L which was attributed to differences in solid solution strengthening from increased silicon and nitrogen content of 316LSi and lower stacking fault energy [5]. The tensile properties of GMA-DED 316LSi are reported to be similar to that of GMA-DED 316H [6]. Future work, such as interrupted creep tests and determination of activation energy to determine the rate-controlling mechanism during creep, is needed to understand the difference in creep performance of 316LSi across the testing temperatures.

Examination of the minimum creep rate to determine the creep stress exponent at 650 °C was done using the Norton Bailey creep model and is shown in Figure 3 [17]. Creep tests at additional stresses was performed for each alloy (not shown in Figure 2) to help determine the stress exponent. The stress

exponents for all the stainless steel alloys fall between 7 and 13 which is consistent with power law glide + dislocation climb creep mechanism reported for wrought 316L [8]. The 316L exhibits the largest minimum creep rates as expected based on the creep curves presented in Figure 2. The 16-8-2 samples tested at 245 MPa failed after approximately 5 hours and exhibited a high minimum creep rate resulting in an inflection in data and indicating power law breakdown occurs for 16-8-2 between 200 – 245 MPa.

Typically, a lower minimum creep rate correlates to longer creep lives assuming similar creep ductility based on the Monkman-Grant relationship [17,18]. 316H exhibits relatively low minimum creep rates which correlates well with the longest reported creep lives at 650 °C shown in Figure 2. This further emphasizes 316H as exhibiting the best creep performance across alloys and testing temperatures making it the top choice for GMA-DED fabrication of power generation components. The 16-8-2 showed the lowest minimum creep rates within power law creep indicating that it should have increased creep performance compared to 316LSi and 316H. However, 16-8-2 samples showed shorter rupture times compared to 316LSi and 316H. For 16-8-2 to exhibit lower minimum creep rates and shorter creep lives than 316LSi it is likely that ferrite formed during tertiary creep and accelerated creep damage locally where it formed. If ferrite formed during the early stages of creep, it would be expected that the minimum creep rates of 16-8-2 would be greater leading to a larger stress exponent than 316LSi. The rupture time, creep ductility, and minimum creep rates of all the stainless steel alloys for all temperatures are reported in Table S-

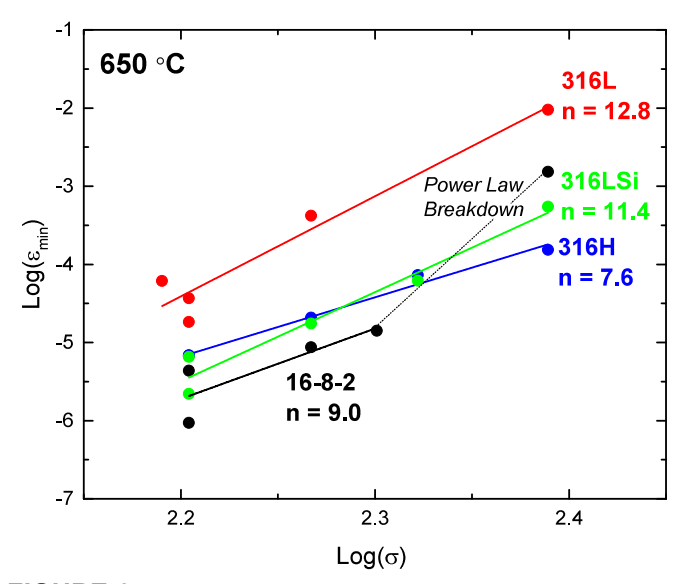


FIGURE 3. PLOT OF LOG(STRESS) VS. LOG (MINIMUM CREEP RATE) FOR 316L, 316LSi, 316H, AND 16-8-2 650 °C CREEP SAMPLES WHERE SLOPE OF EACH LINEAR FIT IS THE CREEP EXPONENT (n) IN THE NORTON-BAILEY CREEP MODEL.

3.2 Creep Damage

Figure 4 shows the macroscopic deformation and creep damage in the different alloys and test conditions. The lower creep ductility in 16-8-2 at 650 °C corresponds to the limited necking and deformation observed in Figure 4d. In general, the creep damage increased as test temperature increased.

BSE micrographs of the creep samples tested at 650 °C and 160 MPa are shown in Figure 5. Void formation along grain boundaries was observed for all samples with a considerable amount of void formation at grain boundary triple points where there is a stress concentration. Negligible intragranular creep damage accumulation was observed. The solution annealing performed on the GMA-DED builds did not result in recrystallization. As such, the grain boundaries where creep damage accumulated were formed during solidification. The damage accumulation at grain boundaries indicates that the remanent intragranular δ -ferrite (Figure 1) which has a propensity to form σ phase is not a significant location for creep damage accumulation.

Subgrains are observed in Figure 5a – c for 316L, 316LSi and 316H. In Figure 5d, a plate-like morphology is observed for 16-8-2 creep sample which obscures imaging of possible subgrains. As reported by DeNonno et al., 16-8-2 has limited austenite stability which results in formation of ferrite during creep and martensite upon cooling after creep testing. The plate morphology shown in Figure 5d is likely martensite. The formation of subgrains during creep, where dislocations arrange themselves into low angle grain boundaries, is associated with power law creep involving dislocation glide and climb [19,20]. The formation of subgrains in the 316L, 316LSi, and 316H samples indicate power law creep is dominant at 650°C and 160 MPa, which matches well with the stress exponent determined from the Norton-Bailey plot in Figure 3. Matthew et al. reported a stress exponent of 9 for wrought stainless steel test at 650 °C which also indicates power law glide + dislocation climb creep mechanism is dominant. For the higher stress conditions below 245 MPa, they observed subgrain formation as well, matching with results reported here [21].

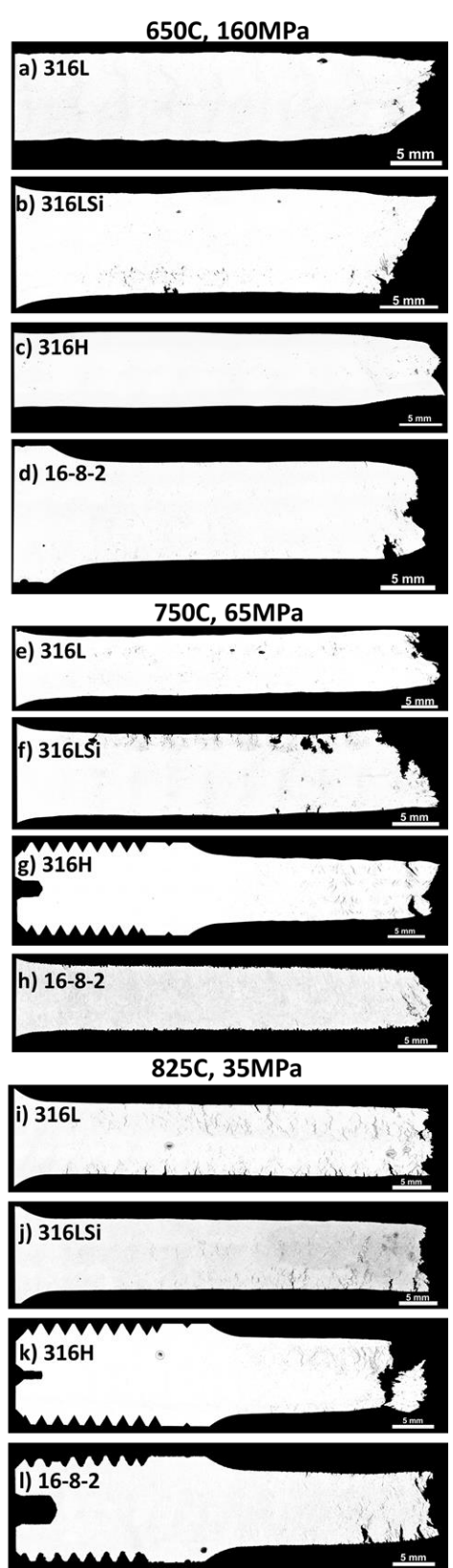


FIGURE 4. OPTICAL MACROGRAPHS OF CREEP SAMPLES TESTED AT 650 °C AND 160 MPA (A-D), 750 °C AND 65 MPA (E-H), AND 825 °C AND 35 MPA (I-L).

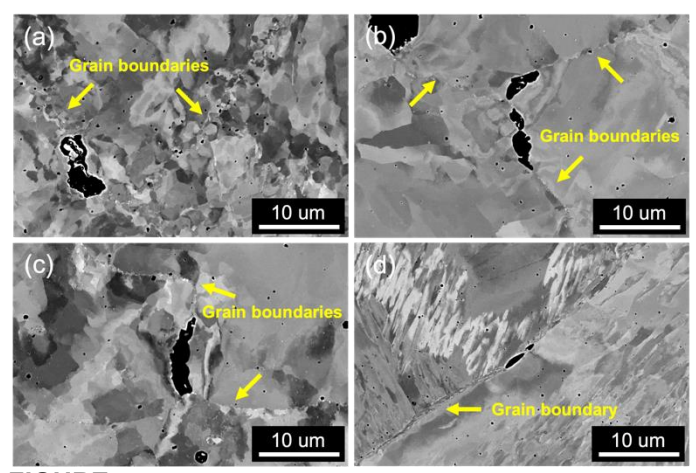


FIGURE 5. BSE MICROGRAPHS OF CREEP SAMPLES TESTED AT 650 °C AND 160 MPa FOR (a) 316L, (b) 316LSi, (c) 316H, AND (d) 16-8-2.

Along with void formation, precipitates were observed decorating grain boundaries as shown by the EDS maps in Figure 6. The EDS maps in Figures 6 correlated to the locations imaged in Figure 5a-d, respectively. The EDS maps indicate the precipitates are rich in chromium, molybdenum, and carbon and depleted in Ni.

Based on the equilibrium phase predictions shown in Table 2 it is possible the precipitates are laves, η , $M_{23}C_6$ carbides, or σ phase. Laves, η , $M_{23}C_6$ are typically rich in chromium and molybdenum, while σ phase is likely enriched with chromium and iron, with smaller amounts of nickel based on the equilibrium phase predictions. The increased enrichment of molybdenum and carbon indicated the precipitates are likely $M_{23}C_6$ as well as possibly small amounts of the other phases (σ , laves and η), however X-ray diffraction of aged samples has identified both σ and $M_{23}C_6$ to be present [6]. The formation of these secondary phases at grain boundaries likely enhances the void formation observed in Figure 5.

3.3 Creep Performance of GMA-DED Builds vs. Wrought 316H

The creep behavior of the GMA-DED austenitic stainless steel samples are compared to wrought 316H in a Larson-Miller plot shown in Figure 7. The solid red line on the plot indicates mean behavior for wrought 316H and the dashed lines indicate the 95% confidence interval. At the higher stress conditions (245 MPa and 200 MPa) at 650 °C 316L, 316LSi, and 16-8-2 samples have smaller Larson-Miller parameter values than wrought 316H, although those testing stresses are near or exceed the yield strength of the GMA-DED alloys. At lower stresses and higher testing temperatures, 316LSi, 316H, and 16-8-2 fall within expected behavior of wrought 316H. The 316L exhibits reduced creep performance at 650 °C compared to wrought 316H but is within range of the expected mean at 750 °C and 825 °C. Overall

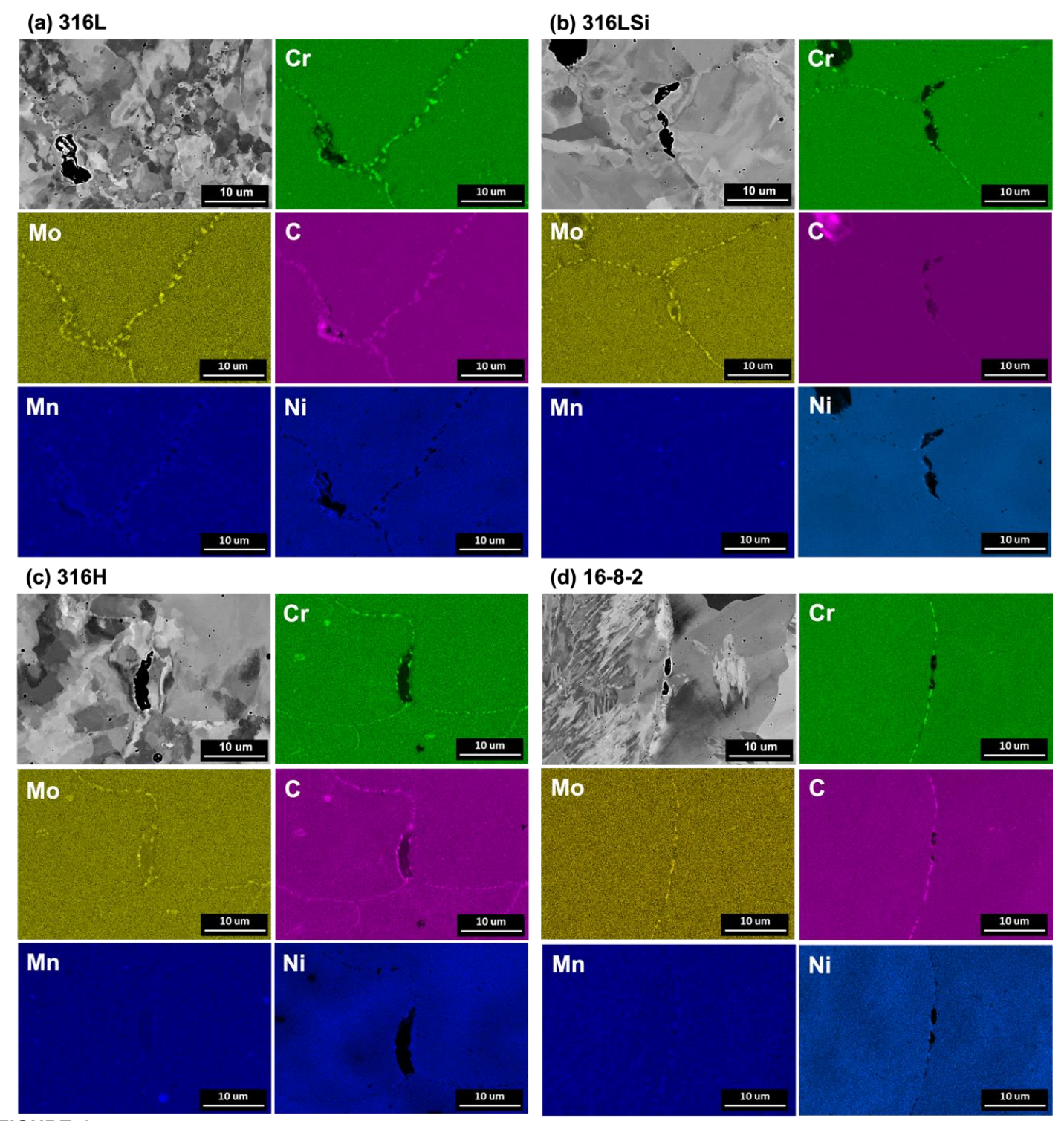


FIGURE 6. EDS MAPS OF DAMAGE AT GRAIN BOUNDARIES OF (a) 316L, (b) 316LSi, (c) 316H, and (d) 16-8-2 CREEP SAMPLES TESTED AT 650 °C AND 160 MPa.

the creep behavior of the GMA-DED alloys is comparable to wrought 316H indicating GMA-DED process can be used to produce parts for creep limited components.

The use of industry standard welding feedstock are feasible for production of parts for high temperature service using GMA-DED process, but it is essential to also understand the long-term microstructure stability. The decreased performance of 16-8-2 shown here may have been previously determined as there is a weld strength reduction factor for Type 316L stainless steel welded with 16-8-2 filler between 510 °C and 649 °C per ASME BPVC Section I [22]. However, the mechanism responsible for the decreased creep performance of 16-8-2 has not been discussed until now, and comparison to cross weld data is of interest for future work. Also consider that most 16-8-2 welds in service are not solution annealed, which may contribute to potential differences in microstructure and performance for solution annealed GMA-DED material relative to cross weld samples.

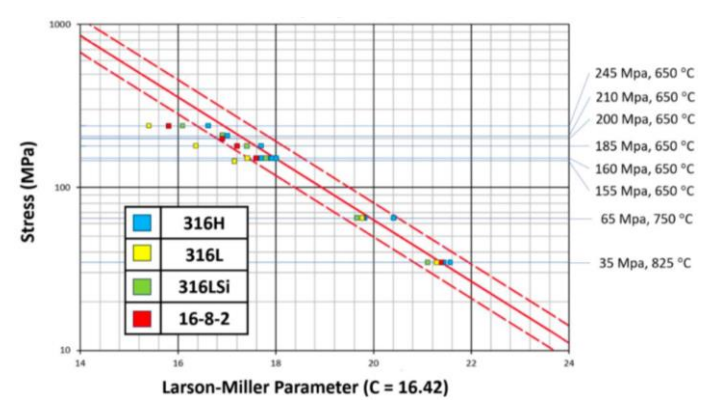


FIGURE 7. LARSON-MILLER PLOT OF GMA-DED 316L, 316LSi, 316H, 16-8-2, AND WROUGHT 316H INDICATED BY RED LINES. THE SOLID RED LINES ON THE PLOT INDICATES MEAN BEHAVIOR FOR WROUGHT 316H AND THE DASHED LINES INDICATE THE 95% CONFIDENCE INTERVAL.

4. CONCLUSION

GMA-DED builds were produced using four austenitic stainless steel welding fillers, 316L, 316LSi, 316H, and 16-8-2. Creep testing was performed at 650 °C, 750 °C and 825 °C and creep damage was investigated. A Larson-Miller plot was used to compare creep performance of the GMA-DED stainless steel alloys to wrought 316H. The conclusions from this study are as follows:

- At 650 °C 316H exhibits the best creep performance followed by 316LSi. 16-8-2 exhibits reduced creep life and creep ductility at 650 °C, likely due to the formation of ferrite during testing. At 750 °C and 825 °C 316H and 16-8-2 exhibit the best creep performance while 316LSi exhibits the worst.
- The Norton-Baily plot indicates stress exponents consistent with power law dislocation glide + climb creep for all alloys at 650 °C.

- Creep damage accumulation at solidification grain boundaries and triple points was observed along with subgrain formation which aligns well with power law dislocation glide + climb being rate controlling mechanism at 650 °C.
- Grain boundary precipitates enriched in chromium, molybdenum, and carbon were observed and are likely M₂₃C₆ carbides as well as σ. The precipitation of secondary particles on grain boundaries likely aids in creep damage accumulation.
- The creep performance of the GMA-DED stainless steel alloys is similar to that of wrought 316H based on the Larson-Miller plot, indicating the GMA-DED process is a viable method for producing creep limited components.

ACKNOWLEDGEMENTS

The authors acknowledge support from the Electric Power Research Institute as well as the Manufacturing and Materials Joining Innovation Center (Ma²JIC), USA.

This material is based upon work supported by the National Science Foundation under Grant Number (2052819).

Data analysis was supported by instrumentation that was acquired through the support of the National Science Foundation (DMR-1828454).

Any opinions, findings, and conclusions or recommendations expressed in this material are those of the author(s) and do not necessarily reflect the views of the National Science Foundation.

AUTHOR CONTRIBUTION

Eun Jang - Conceptualization, Methodology, Formal Analysis, Investigation, Writing – Original Draft, Writing – Review and Editing

Olivia DeNonno: Conceptualization, Methodology, Formal Analysis, Investigation, Writing – Original Draft, Writing – Review and Editing

Juan Gonzales: Methodology, Investigation

Jonah Klemm-Toole: Conceptualization, Methodology, Resources, Writing – Review and Editing, Supervision, Funding Acquisition

Stephen Tate: Conceptualization, Methodology, Resources, Writing – Review and Editing, Supervision, Funding Acquisition

REFERENCES

[1] DebRoy T, Wei HL, Zuback JS, Mukherjee T, Elmer JW, Milewski JO, et al. Additive manufacturing of metallic components – Process, structure and properties. Progress in Materials Science 2018;92:112–224. https://doi.org/10.1016/j.pmatsci.2017.10.001.

[2] American Welding Society (AWS) A5 Committee on Filler Metals and Allied Materials. Welding Consumables—Wire Electrodes, Strip Electrodes, Wires, and Rods for Arc Welding of Stainless and Heat Resisting Steels—Classification. 2016.

- [3] Smith JJ, Farrar RA. Influence of microstructure and composition on mechanical properties of some AISI 300 series weld metals. International Materials Reviews 1993;38:25–51. https://doi.org/10.1179/imr.1993.38.1.25.
- [4] Swanepoel DB, Pistorius PGH. Microstructural changes in 16-8-2 weld metal during exposure to 750 °C for extended times. Weld World 2022;66:301–11. https://doi.org/10.1007/s40194-021-01201-4.
- [5] Hagen L, Yu Z, Clarke A, Clarke K, Tate S, Petrella A, et al. High deposition rate wire-arc directed energy deposition of 316L and 316LSi: Process exploration and modelling. Materials Science and Engineering: A 2023;880:145044. https://doi.org/10.1016/j.msea.2023.145044.
- [6] Gonzalez J, Tate S, Klemm-Toole J. Microstructure and Mechanical Property Stability of Wire Arc Directed Energy Deposition Austenitic Stainless Steels During Thermal Aging at 650°C. JOM 2023;75:4793–807. https://doi.org/10.1007/s11837-023-06120-x.
- [7] Ward AL. Austenitic stainless steel weld materials. A data compilation and review. Hanford Engineering Development Lab n.d.
- [8] Morris DG, Harries DR. Creep and rupture in Type 316 stainless steel at temperatures between 525 and 900°C Part I: Creep rate. Metal Science 1978;12:525–31. https://doi.org/10.1179/msc.1978.12.11.525.
- [9] Ávila Calderón LA, Rehmer B, Schriever S, Ulbricht A, Agudo Jácome L, Sommer K, et al. Creep and creep damage behavior of stainless steel 316L manufactured by laser powder bed fusion. Materials Science and Engineering: A 2022;830:142223. https://doi.org/10.1016/j.msea.2021.142223.
- [10] Li Y, Krajňák T, Podaný P, Veselý J, Džugan J. Thermal stability of dislocation structure and its effect on creep property in austenitic 316L stainless steel manufactured by directed energy deposition. Materials Science and Engineering: A 2023;873:144981.

https://doi.org/10.1016/j.msea.2023.144981.

- [11] Williams RJ, Al-Lami J, Hooper PA, Pham M-S, Davies CM. Creep deformation and failure properties of 316 L stainless steel manufactured by laser powder bed fusion under multiaxial loading conditions. Additive Manufacturing 2021;37:101706. https://doi.org/10.1016/j.addma.2020.101706.
- [12] A01 Committee. Specification for General Requirements for Flat-Rolled Stainless and Heat-Resisting Steel Plate, Sheet, and Strip. ASTM International; n.d. https://doi.org/10.1520/A0480_A0480M-22A.
- [13] E01 Committee. Test Method for Analysis of Austenitic Stainless Steel by Spark Atomic Emission Spectrometry. ASTM International; n.d. https://doi.org/10.1520/E1086-14.
- [14] E01 Committee. Test Methods for Determination of Carbon, Sulfur, Nitrogen, and Oxygen in Steel, Iron, Nickel, and Cobalt Alloys by Various Combustion and Fusion Techniques. ASTM International; n.d. https://doi.org/10.1520/E1019-18.

- [15] Sherby OD, Burke PM. Mechanical Behavior of Crystalline Solids at Elevated Temperature. Progress in Materials Science 1968:13:323–90.
- [16] DeNonno O, Gonzales J, Tate S, Hamlin R, Klemm-Toole J. Role of Austenite Stability in Elevated Temperature Mechanical Properties of Gas Metal Arc Directed Energy Deposition Austenitic Stainless Steels. JOM (In Review) n.d.
- [17] Kassner ME. Fundamentals of creep in metals and alloys. 3. ed. Amsterdam [u.a.]: Elsevier; 2015.
- [18] Dobeš F, Milička K. The relation between minimum creep rate and time to fracture. Metal Science 1976;10:382–4. https://doi.org/10.1080/03063453.1976.11683560.
- [19] Challenger KD, Moteff J. Quantitative characterization of the substructure of AISI 316 stainless steel resulting from creep. Metall Trans 1973;4:749–55. https://doi.org/10.1007/BF02643084.
- [20] Kestenbach H-J, Luiz Da Silvelra T, Monteiro SN. On subgrain formation during creep of 316 stainless steel. Metall Trans A 1976;7:155–8. https://doi.org/10.1007/BF02644054.
- [21] Mathew MD, Sundararaman M, Mannan SL. Dislocation Substructure and Precipitation in Type 316 Stainless Steel Deformed in Creep. Mater Trans, JIM 1997;38:37–42. https://doi.org/10.2320/matertrans1989.38.37.
- [22] BPVC Section I-Rules for Construction of Power Boilers. ASME; 2023.

SUPPLEMENTAL MATERIAL

TABLE S-1. SUMMARY OF CREEP RUPTURE TIME, CREEP DUCTILITY, AND MINIMUM CREEP RATE FOR GMA-DED STAINLESS STEEL ALLOYS CREEP TESTED AT 650 °C, 750 °C, 825 °C.

Alloy	Temperature (°C)	Stress (MPa)	Rupture Time (Hours)	Creep Ductility	E _{min} (%/s)
316L		155	125.9	33%	6.1 x 10 ⁻⁵
		160	452.5	69%	1.8 x 10 ⁻⁵
	650 °C	160	278.2	58%	3.7 x 10 ⁻⁵
		185	19.6	35%	4.2 x 10 ⁻⁴
		245	1.74	43%	9.5 x 10 ⁻³
	750 °C	65	788.9	43%	1.1 x 10 ⁻⁵
	825 °C	35	891.4	18%	1.6 x 10 ⁻⁶
316LSi		160	819	38%	6.6 x 10 ⁻⁶
		160	1326.9	48%	2.2 x 10 ⁻⁶
	650 °C	185	291.5	26%	1.7 x 10 ⁻⁵
		210	92.1	27%	6.2 x 10 ⁻⁵
		245	11.7	37%	5.5 x 10 ⁻⁴
	750 °C	65	684.8	39%	2.6 x 10 ⁻⁶
	825 °C	35	621.4	17%	2.6 x 10 ⁻⁶
316H		160	1092.9	19%	1.8 x 10 ⁻⁶
	650 °C	160	956.4	41%	3.4 x 10 ⁻⁶
		185	641.1	40%	2.1 x 10 ⁻⁵
		210	113.3	36%	7.3 x 10 ⁻⁵
		245	37.1	27%	1.5 x 10 ⁻⁴
	750 °C	65	906.1	34%	3.9 x 10 ⁻⁶
	825 °C	35	1088.6	15%	5.0 x 10 ⁻⁷
16-8-2		160	496.3	11%	1.7 x 10 ⁻⁶
	650 °C	160	738.6	12%	9.4 x 10 ⁻⁷
		185	179.6	14%	8.7 x 10 ⁻⁶
		200	88.3	12%	1.4 x 10 ⁻⁵
		245	5.2	22%	1.5 x 10 ⁻³
	750 °C	65	1774.8	33%	4.2 x 10 ⁻⁶
•	825 °C	35	1148.3	17%	1.75 x 10 ⁻⁶